From elasticity to capillarity in soft materials indentation

Jonathan T. Pham, Frank Schellenberger, Michael Kappl,* and Hans-Jürgen Butt
Max Planck Institute for Polymer Research, Ackermannweg 10, 55128 Mainz, Germany
(Received 20 February 2017; revised manuscript received 30 April 2017; published 19 June 2017)

For soft materials with Young's moduli below 100 kPa, quantifying mechanical and interfacial properties by small scale indentation is challenging because in addition to adhesion and elasticity, surface tension plays a critical role. Until now, microscale contact of very soft materials has only been studied by static experiments under zero external loading. Here we introduce a combination of the colloidal probe technique and confocal microscopy to characterize the force-indentation and force-contact radius relationships during microindentation of soft silicones. We confirm that the widespread Johnson-Kendall-Roberts theory must be extended to predict the mechanical contact for soft materials. Typically a liquid component is found within very soft materials. With a simple analytical model, we illustrate that accounting for this liquid surface tension can capture the contact behavior. Our results highlight the importance of considering liquid that is often associated with soft materials during small scale contact.

DOI: 10.1103/PhysRevMaterials.1.015602

I. INTRODUCTION

Micro- and nanoscale contact between two solid bodies is ubiquitous throughout nature as well as in manufacturing, technology, and materials characterization. For example, many climbing organisms generate small contact points with their counterpart surface, making small scale contact mechanics important for the development of bioinspired adhesives [1–3]. In mechanobiology, cell-cell and cell-surface forces are essential elements in understanding tissue development, where contact points are on cellular to subcellular length scales [4–6]. From an industrial perspective, processability and manufacturing of cosmetic, food, and pharmaceutical products hinges upon understanding the adhesion between micro- and nanoscale particles in cohesive powders [7,8].

A common model system to study small contact is a spherical microparticle indenting a flat plane. Taking into account deformation and adhesion of the two interacting surfaces, the Johnson-Kendall-Roberts (JKR) theory describes the contact mechanics by relating external force (F), contact radius (a), and indentation depth (δ) [9]. Johnson, Kendall, and Roberts demonstrated that even under zero external load, a gain of interfacial energy in the contact zone establishes a finite contact area between two rubber spheres. Since then, the JKR theory has become a staple in characterizing mechanical properties and adhesion of soft materials [10–23].

For super soft or biological materials with Young's moduli (E) on the order of a few kilopascals, JKR theory breaks down on small scales [24–27]. This discrepancy has been linked to surface stress (Υ), which is the energy required to create new surface by stretching the interface [25–34]. When the particle radius (R) is similar in size to the elastocapillary length, $L_{EC} = \Upsilon/E$, surface stress is non-negligible and must be taken into account. For soft materials with $E \sim 10^2$ to 10^6 Pa, L_{EC} ranges from ~50 nm to 0.5 mm.

By placing microparticles on soft polydimethylsiloxane (PDMS), Style *et al.* showed that the relationship between a or δ with R can be explained when accounting for solid surface stress [25,29]. Although recently, Jensen *et al.* demonstrated that untethered liquid silicone molecules separate from the solid PDMS network [36], adding another complication to the contact behavior associated with liquid surface tension. To date, experiments have been restricted to the special case of zero external loading; a and δ have only been measured for static particles on a surface. This is likely because of the difficulty in implementing visualization with force and indentation measurements on small length and force scales. However characterization of local mechanical and interfacial properties is often achieved by applying forces and indentations while making assumptions on a or δ.

Here, we address this experimental challenge by combining the colloidal probe technique with confocal microscopy to measure the force associated with indenting a rigid microsphere into a soft PDMS surface while simultaneously visualizing the contact radius [Fig. 1(a)]. Our approach offers high force sensitivity and the ability to capture a cross-sectional image of the contact to measure both a and δ. We show through our experiments and a simple analytical model that in addition to the contribution of surface stress, which has been previously reported in the literature, an additional contribution for liquid surface tension needs to be considered. In nearly all soft silicone materials, a liquid component is found within the material that plays a significant role at small length scales. Our results are important for mechanical characterization of soft materials, for example in determining local elastic moduli by atomic force microscopy. Moreover, our experimental approach offers a unique quantitative method towards understanding indentation, adhesion, and separation of small scale contacts.

II. RESULTS AND DISCUSSION

A. Measuring force, indentation, and contact radius

For our experiments, a silica particle of radius $R \approx$ 4–6.5 μm is used to indent a PDMS elastomer. We tune the Young's modulus of the material by controlling the ratio of silicone base and crosslinking agent to 20:1, 40:1, 50:1, and 60:1 by weight, leading to nominal values for the moduli of

*kappl@mpip-mainz.mpg.de

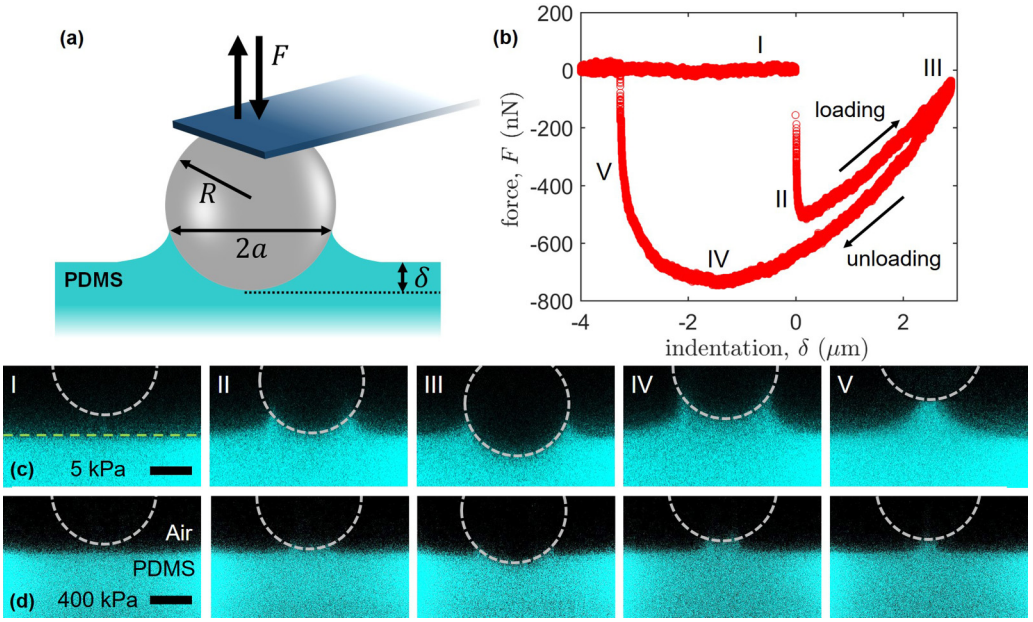

FIG. 1. Measuring force, indentation, and contact geometry of soft solid surfaces. (a) Schematic of a colloidal probe in contact with a soft solid surface. The relevant parameters of force F, contact radius a, indentation δ, and the particle radius R are labeled. (b) A representative force-indentation curve measured by AFM indentation on PDMS with $E_{\text{bulk}} = 5$ kPa and a maximum indentation depth $\delta \approx 2.8$ μm. (c) Corresponding cross-sectional images obtained by confocal microscopy of the labeled points on the force-indentation curve in part (b). The green dashed line represents the interface between solid and air, which is determined by measuring reflection at the surface (Fig. S2 [35]). The gray circle represents the spherical probe as a guide to the eye. (d) Confocal images of indentation on PDMS with $E_{\text{bulk}} = 400$ kPa, illustrating the clear difference in contact deformation. Note that image III in (d) is not the maximum indentation but rather the same force as in (c) during retraction for comparison. The particle radius here is $R = 6.5$ μm. Scale bars: 5 μm.

$E_{\text{bulk}} \approx 400$, 40, 15, and 5 kPa, respectively. These values are measured by both uniaxial tensile testing and shear rheology on macroscopic samples at low strain rate (Fig. S1 [35]). The PDMS film thickness is $h \sim 30$ μm, which leads to $\delta/h \sim 0.1$ and a maximum $a/h \sim 0.2$. Since these ratios are small, the finite thickness is neglected here [21,37–39].

During a continuous indentation experiment, the colloidal probe cantilever base is moved at a constant rate of 100 nm/s towards the substrate. Upon contact, the particle is further indented into the material to a set indentation depth δ. It is then retracted until the particle detaches from the substrate and reaches the initial position. Indentation is taken relative to the flat surface prior to contact (Fig. S2 [35]). To extract δ from the cantilever position, the cantilever deflection is subtracted from the base displacement. Positive forces and indentations indicate repulsion and indentation into the surface while negative values represent an attractive force and stretching of the material. An example of a measured force-indentation curve is presented in Fig. 1(b) for a 5 kPa sample. Images corresponding to the numbered regions in the F vs δ curve are given in Fig. 1(c). In comparison, the contact radius and indentation on a 400 kPa surface are much smaller at the same loading [Fig. 1(d)].

The dependence of the normalized contact radius a/R, measured by confocal imaging, is presented in Figs. 2(a) and 2(b) as a function of the normalized indentation depth δ/R, and normalized force F/R, measured by AFM. F-δ curves of the four moduli are given in Fig. S3 [35]. As a sample is indented, the contact radius naturally increases [Fig. 2(a)]. Upon retraction, the contact radius is larger than during the approach due to adhesion. Even for negative indentation, the contact radius remains finite since the PDMS stretches. As the modulus is decreased, the contact radius systematically increases for a given indentation depth because the substrate has lower resistance to deformation. For the 5 kPa material, a approaches R for higher indentations (red circles). Figure 2(b) demonstrates that increase of the normalized contact radius as a function of the normalized load is faster for very soft surfaces. a/R approaches unity at a force of ~200 nN ($F/R \approx 0.03$) for the 5 kPa sample while a/R reaches only ~0.35 at the same loading for the 400 kPa PDMS.

B. Quasistatic step and hold measurements

In the above experiments, we demonstrate the general trend of increasing contact radius and increasing adhesion with decreasing moduli. However, force-indentation curves are rate dependent due to the viscoelastic nature of PDMS (Fig. S5 [35]). This behavior is further complicated by the rate dependent formation/breaking of the interface [14,40,41], as well as possible poroelastic effects [42]. To further analyze how indentation depends on rate, we conduct step and hold experiments to allow for force relaxation (Fig. 3).

In these experiments, the colloidal probe is indented approximately 500 nm into the material and held for 15 minutes before being indented to the next step. The average indentation

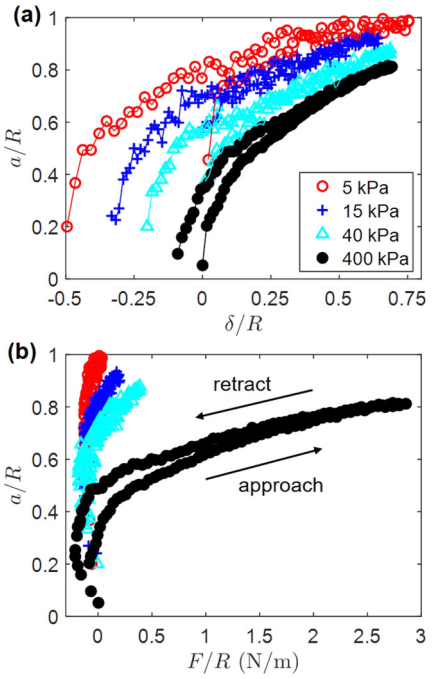

FIG. 2. Contact radius as a function of indentation and force for different moduli. (a) Contact radius as a function of indentation depth (both normalized by the particle radius $R = 6.5$ μm), illustrating the rate at which a/R approaches unity for different moduli (5, 15, 40, and 400 kPa). (b) Normalized contact radius vs normalized load, illustrating the rate at which a/R increases with force for different moduli. See Fig. S4 [35] for retraction only and a zoomed in force range.

rate is of the order of $\delta/900$ s $\sim$ 1 nm/s. AFM indentation depth and confocal images are consistent and stable over 15 minutes (Fig. 3). The contact radius is simultaneously measured and plotted in Fig. 3 as an average of the last five minutes of the holding step. The contact radius is constant with little fluctuation after 10 minutes, permitting a to be taken over the last five minutes to minimize error. For the 400 kPa sample, the force reaches a plateau on all approaching indentations [Fig. 3(a), i and ii]. For the 5 kPa sample, positive indentations also reach a plateau; the variation in force is $\sim$2 nN over the last five minutes [Figs. 3(b) i and 3(b) ii]. For these insets, the x axis scale is kept constant at 16 minutes and the y axis at 1 μN (400 kPa) and 100 nN (5 kPa) for comparison. During pull out steps on the 400 kPa sample, the force relaxes and reaches a plateau [Fig. 3(a) iii]. The particle detaches from the surface during a third 1.5 μm retraction step. In contrast, many 1.5 μm retraction steps are required to detach the particle from the 5 kPa surface. For early retraction steps, the force reaches a plateau [Fig. 3(b) ii]. However for later retraction steps, the force does not stabilize over the 15 minute hold [Fig 3(b), iii], even though the contact radius remains constant. In the last step of Fig. 3(b), the hold time was set to 45 minutes. Even then the particle stays attached but the force does not stabilize. Therefore, in the following quantitative analysis, we only consider holding steps where the force has reached a plateau in the last five minutes. Since the force does not reach a plateau on highly retracted pull out steps, they are not suitable for a rate-independent analysis and not considered here.

C. Modulus from AFM-confocal experiments

For materials characterization, Young's moduli can be determined by fitting JKR theory to indentation experiments. We compared modulus values obtained by JKR theory on our indentations, denoted as E_{JKR}, to bulk measured values, E_{bulk} (Fig. S1 [35]). Since modulus is a material property, it is independent of the testing method and E_{JKR} must be equal to E_{bulk}. According to JKR theory for a rigid sphere indenting an elastic half space, the external force is related to the contact radius and indentation as:

$$F_{\mathrm{JKR}} = 2E^* a\left(\delta - \frac{a^2}{3R}\right) = E_{\mathrm{JKR}}\left(\frac{8a\delta}{3} - \frac{8a^3}{9R}\right). \quad (1)$$

Note that the effective elastic modulus has been taken as $E^* = 4E_{\mathrm{JKR}}/3$ for an incompressible solid. By plotting the measured force F vs $8a\delta/3 - 8a^3/9R$ [Figs. 4(a) and 4(b)], one expects a linear trend with the slope giving E_{JKR} [Eq. (1)]. As expected, our results show a linear behavior and the modulus is directly extracted by a linear fit. For the 400 kPa PDMS, JKR theory predicts a modulus of $E_{\mathrm{JKR}} = 397 \pm 43$ kPa, which is consistent with E_{bulk}. For the 40, 15, and 5 kPa materials, the modulus values determined by JKR are $E_{\mathrm{JKR}} = 66 \pm 6, 33 \pm 1, 15 \pm 2$ kPa, respectively. The moduli are systematically overestimated when compared to the bulk mechanical testing by factors of $E_{\mathrm{JKR}}/E_{\mathrm{bulk}} \approx 1.7$, 2.2, and 3.0, respectively [Fig. 4(b)]. It is worth pointing out that although the linear trends are consistent with Eq. (1) for all of the moduli tested, the E_{JKR} values are inconsistent with E_{bulk} for the three softer PDMS.

To visualize how JKR fits to the F-δ relationship, we plot experimental results and overlay calculated values of F_{JKR} from Eq. (1) for approach and retract data of the 400 and the 5 kPa substrates [Figs. 4(c) and 4(d)]. Good agreement between JKR and our experimental results is observed for the 400 kPa PDMS [Fig. 4(c)]. Curves plotted using $E_{\mathrm{bulk}} =$ 400 kPa overlay experiments well. This is not the case for the soft, 5 kPa PDMS [Fig. 4(d)], demonstrating that JKR theory does not describe the contact mechanics for very soft materials. Similar plots for the 40 and 15 kPa surfaces are presented in Fig. S6 [35]. Note that the positive indentations overlap quite well in the approach and retraction directions, justifying a rate-independent analysis.

For soft PDMS, particularly with the 5 kPa modulus, measuring small contact radii is not possible with a small spherical glass probe because on first contact, the material pulls up around the particle. Since JKR theory was developed under the assumption of small contact radius, it is expected to breakdown in this regime where the contact deformation is large. Although suprisingly JKR theory has been demonstrated to be accurate to reasonably large contact radii [29,43]. In addition, JRK theory invokes an approximation of a parabolic contact geometry, which is only a reasonable approximation for small a. Maguis extended JKR theory to include a large contact radius and the force can be described as [44]:

$$F_{\mathrm{Maugis}} = \frac{8aE}{3}\left(\delta - \frac{R}{2} + \frac{R^2 - a^2}{4a}\ln\frac{R+a}{R-a}\right). \quad (2)$$

However, as illustrated in Fig. 4(d), this extension also does not capture the force-indentation data. In particular,

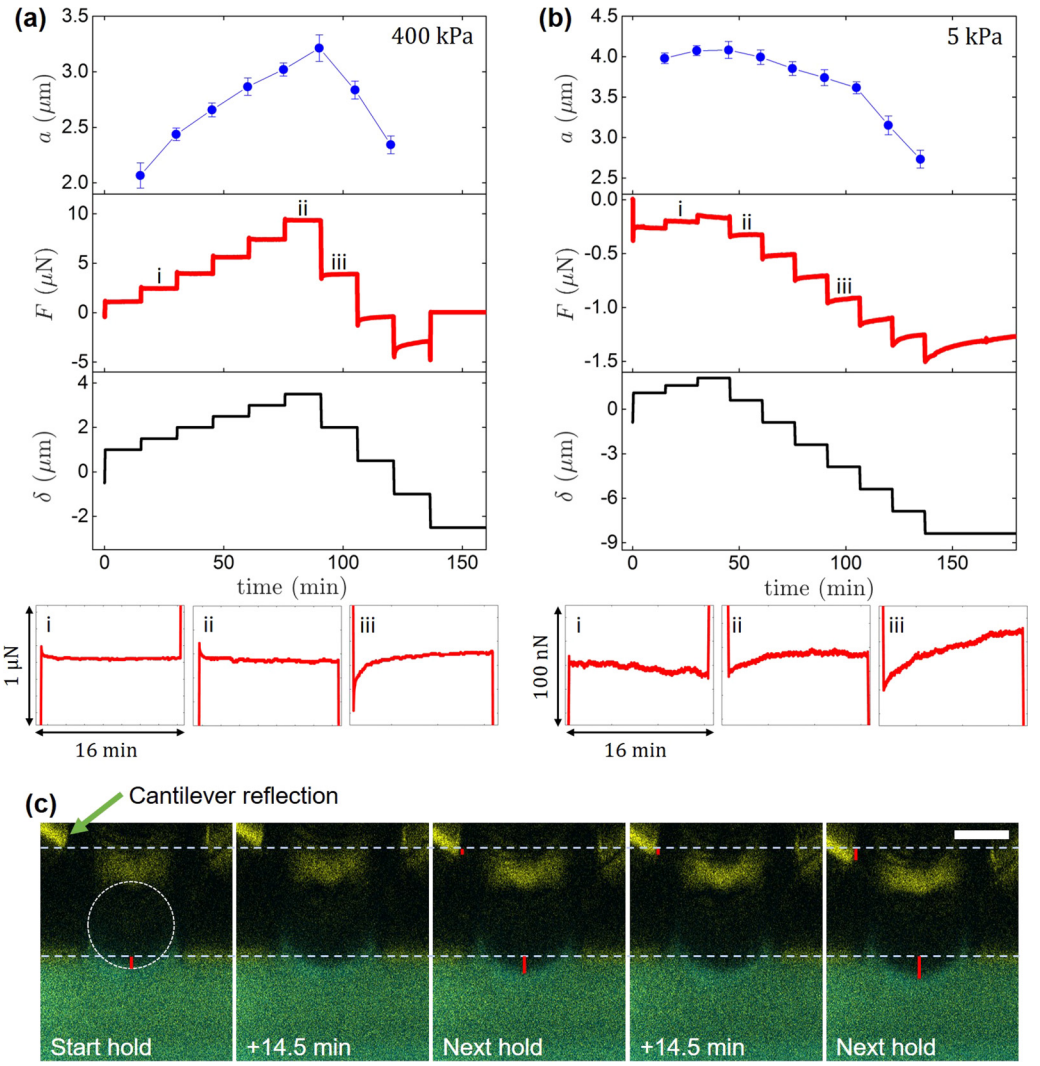

FIG. 3. Quasistatic force-indentation measurements. Contact radius a, force F, and indentation δ as a function of time for the (a) 400 kPa and (b) 5 kPa samples. Each holding step has a duration of 15 minutes. Indentations steps are 500 nm and retraction steps are 1.5 μm. Plots i, ii, and iii are zoomed in F vs time plots to illustrate the different regimes of the labeled indentations. The x axis is 16 minutes and the y axis is 1 μN for (a) and 100 nN for (b). Error bars on the contact radius are standard deviations of measured contact radii over the last five minutes of the holding step. (c) Snapshots of 1.1, 1.6, and 2.1 μm indentation depths for a 15 kPa sample. The bottom dotted line represents the flat surface. The top dotted line is a reference to illustrate the motion of the cantilever (in yellow). Vertical red lines are the expected distances of the cantilever and indentation into the surface, respectively. The circle represents the spherical probe as a guide to the eye. Note the yellow reflection channel brightness is strongly increased for visualization of the cantilever distance at the expense of resolution. The particle radius is $R = 4$ μm. Scale bar: 5 μm.

our measured forces are consistently shifted in the negative direction for softer materials [Figs. 4(d) and S6]. In addition to the contact geometry, JKR theory assumes that the material is linear elastic. In macroscopic mechanical measurements, the 5 kPa material remains linear up to 150% (Fig. S1 [35]).

D. Capillary contribution

Our results illustrate how JKR theory fails in quantitatively predicting the contact mechanics below $E_{\text{bulk}} = 40$ kPa when using a $R \sim 5$ μm indenter. This is consistent with the study of Style *et al.* of static microparticles on a 3 kPa PDMS surface under zero load [25]. In their analysis, they added the contribution of solid surface stress to the elastic and adhesive energies, as accounted for by JKR. This additional contribution was able to describe their results well. However, very soft PDMS is typically a gel; it is a crosslinked network with a penetrating liquid. The liquid in this case is free PDMS chains (i.e., silicone oil) which have not been tethered to the polymer network during crosslinking [36,45]. By solvent extraction in hexane, we quantified the fraction of untethered chains to be as high as ~45% for the 5 kPa PDMS (Fig. S7 [35]). By conducting experiments of static microparticles soft PDMS, Jensen *et al.* recently demonstrated that liquid in the material separates from the polymer network near the contact line [36].

Based on this knowledge, the forces measured in indentation experiments should be associated with capillary forces induced by the free mobile chains. Our experiments illustrate

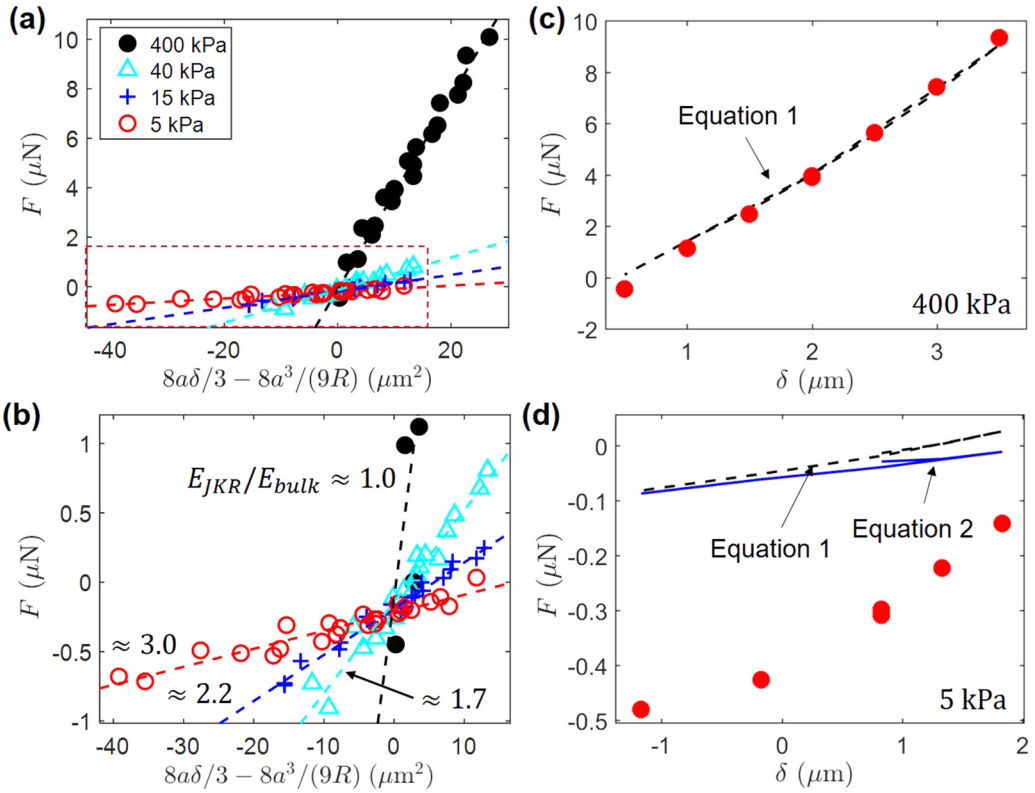

FIG. 4. Comparison of experiment with theory. (a) Measured force as a function of contact radius and indentation depth for quasistatic experiments after 15 minute holds. Dashed lines are linear fits, which provide modulus values (E_{JKR}) predicted by JKR from Eq. (1). (b) A zoomed-in plot of the red dashed boxed in part (a) of the lower modulus curves to illustrate linear behavior. As the material gets softer, the discrepancy between E_{JKR} and E_{bulk} systematically increases. Parts (a) and (b) show the results of three independent experiments for each modulus. (c) Plot of force vs indentation of experimental data (red points) for the 400 kPa PDMS and the JKR fit (dashed line) for approach and retract directions. (d) Similar plot to part (c) for the 5 kPa PDMS but also including the Maugis extension in Eq. (2) (blue line). The particle radius is $R = 4\ \mu$m.

an important concept in the measured force during indentation experiments of soft PDMS: a negative force during positive indentations [Figs. 4(d) and S6]. For a particle indenting into a liquid layer, capillary forces will lead to a negative force pulling down on the particle [46]. Thus, to describe contact for very soft PDMS, we propose a model that includes a contribution from liquid capillarity of the free PDMS chains. Capillary forces (F_{cap}) are caused by capillary pressure and the direct action of surface tension as $F_{\mathrm{cap}} = F_{cp} + F_{\gamma}$. The capillary pressure term is given by $F_{cp} = \pi a^2 \Delta P$, where $\Delta P = \gamma(1/a - 1/r)$, γ is the surface tension of untethered free chains, and r is the meniscus radius of curvature [47]. Since both the contact radius a and the meniscus radius r are of the same order of magnitude and both are several microns, the capillary pressure term is assumed to play little role. Consequently, the capillary force is dominated by the direct action of surface tension. This is expressed as $F_{\gamma} = 2\pi\gamma a \sin\beta$, where β is the angle relative to the horizontal of the PDMS/air interface at the contact line [Fig. 5(a)].

A surface stress term arises from stretching of the solid interface in the contact zone [Fig. 5(a)], as presented by others [25,34,48]. Following these approaches and assuming surface stress is constant and isotropic [25,29], the force for stretching is $F_{\mathrm{stretch}} = 2\pi\Upsilon\delta$. This assumes that the contact zone has a spherical cap geometry with a depth δ and radius R and the surfaces stress of the free solid is equal to the interfacial stress. In reality, the solid/particle interface is likely larger due to the formation of an adhesive ridge. This force scales with the indentation plus a value $c(\delta)$. Here $c(\delta)$ is similar to the observable ridge height (h_a) except that it only includes the fully crosslinked portion of the adhesive ridge [Fig. 5(a)]. It is important to note the difference between these two heights since one is associated with surface stress Υ of the solid and the other with surface tension γ of the free chains. Accordingly, the total force is approximated as the combined contributions of elastic deformation and adhesion from JKR, stretching within the contact zone, and the capillary forces pulling on the sphere as $F_{\mathrm{total}} = F_{\mathrm{JKR}} + F_{\mathrm{stretch}} + F_{\mathrm{cap}}$:

$$F_{\mathrm{total}} = \frac{8Ea\delta}{3} - \frac{8Ea^3}{9R} + 2\pi\Upsilon(\delta + c(\delta)) - 2\pi\gamma a \sin\beta \qquad (3)$$

When γ and Υ are negligible, this recovers JKR. To fit our experiments to Eq. (3), a couple approximations are made. Because we are not able to determine the value $c(\delta)$ experimentally, this value is set to $c(\delta) = 0$. Physically, this approximates the stretched geometry as a spherical cap governed only by the indentation depth. The angle β is approximated as 90°. Since silicone oils completely wet glass [36,49], β reaches 90° at the particle midline and ranges up

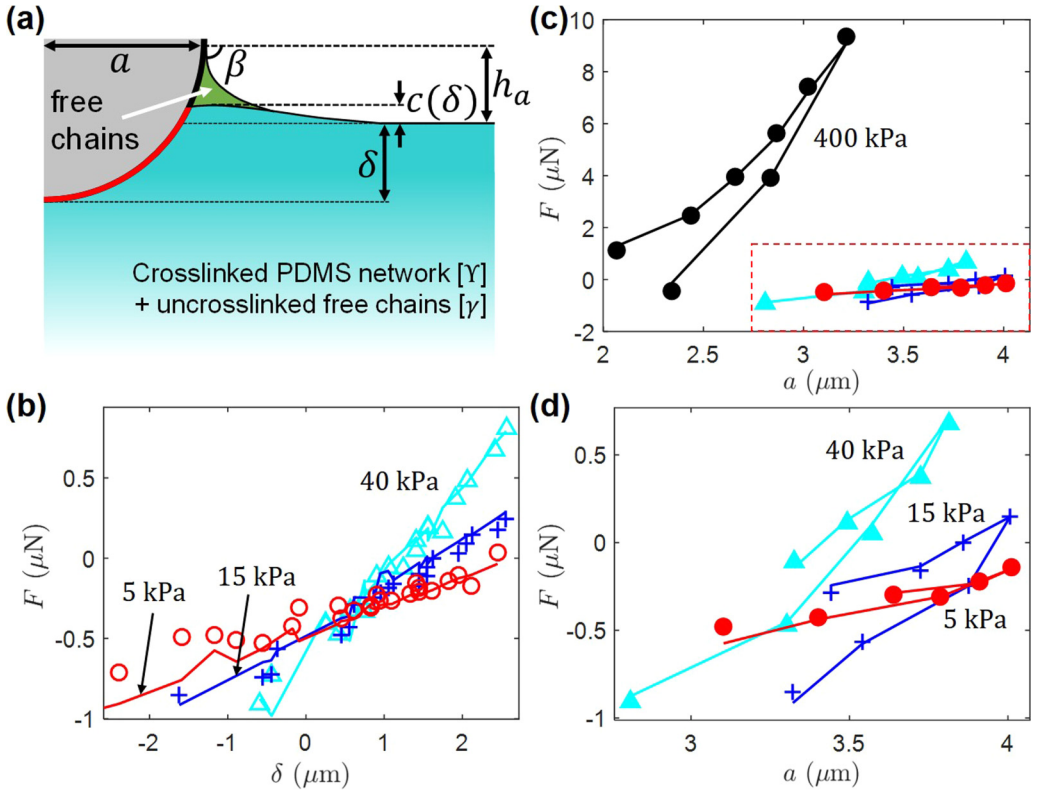

FIG. 5. Including a capillary correction to the force-indentation relationship. (a) Schematic illustrating the relevant variables for Eq. (3). The red line denotes the surface associated with Υ. (b) F vs δ for the three softest materials with best fit γ and Υ and with the modulus fixed to E_{bulk}. The kinks in the fit curves arise because F_{total} is calculated with measured a and δ using three experiments for each modulus. The particle radius is $R = 4$ μm. (c) F vs a for the 400, 40, 15, and 5 kPa PDMS. (d) Zoom-in of the red box of part c for the lower moduli PDMS. The lines are calculated values using Eq. (3). For Figs. 5(c) and 5(d), single experiments are plotted for clarity.

to $\sim$120° for lower contact lines. Then with full knowledge of applied force F, contact radius a, and indentation δ, we find that the addition of capillary forces in Eq. (3) well captures the experimental results.

Using Υ and γ as parameters, experimental results are fit to Eq. (3). The modulus is fixed to measured E_{bulk} and δ and a are measured from our AFM-confocal experiments. Overlaying calculated F_{total} with measured F reveals good agreement [Fig. 5(b)]. The γ values are 20, 19, 15, and 17 mN/m for the 400, 40, 15, and 5 kPa samples, respectively. This gives an average surface tension of $\gamma = 18 \pm 2$ mN/m, which is reasonable for typical surface tension of PDMS oil ($\sim$20 mN/m) [50]. In addition to the F-δ relationship, Eq. (3) also fits well to experimental F-a results [Figs. 5(c) and 5(d)]. We note that without the liquid surface tension term (i.e., only $F_{\text{JKR}} + F_{\text{stretch}}$), the experimental results do not fit well (Fig. S8 [35]).

To better interpret the effect of surface stress, we fit the surface stress Υ to multiple experiments while keeping γ and E_{bulk} constant. For the 400 kPa PDMS, elasticity dominates and Υ plays an insignificant role. This is consistent with the 400 kPa PDMS results agreeing with JKR theory [Fig. 4(c)]. For the softer substrates, surface stress becomes strong enough to balance elasticity and the effect of Υ becomes more pronounced. By fitting the Υ to multiple experiments, we find that the surface stress term increases with the modulus, which yields $\Upsilon = 37 \pm 5$, 29 ± 2, and 18 ± 3 mN/m for the 40, 15, and 5 kPa samples, respectively. Because surface stress is associated with the energy required to create new surface by stretching, it intuitively increases with modulus. Although the fit values of 37 and 29 mN/m may be overestimated due to challenges in experimentally measuring $c(\delta)$, the liquid separation volume, and the local strain, they are within range of previously reported solid surface stress values [25,28,29,51,52], while 18 mN/m is similar to liquid PDMS surface tension. This suggests a transition to where surface tension of the untethered components outweighs the effect of surface stress.

III. SUMMARY

In summary, we combine the colloidal probe technique with confocal microscopy to measure the force, indentation depth, and contact radius while indenting a soft polymer with a rigid, microscale particle. We have confirmed that JKR theory and Maugis' extension to large contact radii are not capable of quantitatively capturing force-indentation data near the elastocapillary length. Importantly, JKR theory can appear suitable for determining a soft material's elastic modulus by fitting linearly to Eq. (1) [Figs. 4(a) and 4(b)]. However, it does not yield accurate values and does not capture the force-indentation relationship. Discrepancy with JRK has been addressed in previous literature by the introduction of a surface stress term that accounts for creating new surface

by stretching the soft solid interface. While this captures zero-load experiments well, it is not able to describe our force-indentation results. With the knowledge of phase separation occurring near the contact line, we have introduced a liquid surface tension term that fits to the experiments.

Our results illustrate a transition from elasticity-dominated (400 kPa) to intermediate (40 and 15 kPa) to capillary-dominated (5 kPa) contact, displaying the requirement of considering liquid components in soft materials near the elastocapillary length. Similar transitions have been proposed theoretically for homogeneous soft solids [32,48]. For the softest material in our study, $L_{EC} \approx 0.02/5000 \approx 4\ \mu$m, which is the particle radius used for our quasistatic experiments (Fig. 3). For the 15 and 40 kPa PDMS, $L_{EC} \sim 1.5\ \mu$m, which is similar in magnitude to our particle radius R. On the other hand, $L_{EC} \sim 0.1\ \mu$m for the 400 kPa material, which is an order of magnitude smaller than R and for this case, the results fit well to JKR theory. Future studies should focus on a better understanding of the interplay between polymeric/oligomeric network components associated with solid and liquidlike behavior and routes to quantify the liquid/solid separation near the contact line during a force-indentation measurement.

ACKNOWLEDGMENTS

We thank Doris Vollmer for stimulating discussions and Sebastian Stappert for kindly providing the dye. We acknowledge support from an Alexander von Humboldt Fellowship (J.T.P.) and an ERC Advanced Grant No. SUPRO 340391 (H.J.B.).

[1] L. F. Boesel, C. Greiner, E. Arzt, and A. del Campo, Adv. Mater. **22**, 2125 (2010).
[2] S. Y. Yang, E. D. O'Cearbhaill, G. C. Sisk, K. M. Park, W. K. Cho, M. Villiger, B. E. Bouma, B. Pomahac, and J. M. Karp, Nat. Commun. **4**, 1702 (2013).
[3] L. Xue, J. T. Pham, J. Iturri, and A. del Campo, Langmuir **32**, 2428 (2016).
[4] J. Kashef and C. M. Franz, Dev. Biol. **401**, 165 (2015).
[5] Z. Liu, J. L. Tan, D. M. Cohen, M. T. Yang, N. J. Sniadecki, S. A. Ruiz, C. M. Nelson, and C. S. Chen, Proc. Natl. Acad. Sci. USA **107**, 9944 (2010).
[6] J. T. Pham, L. Xue, A. del Campo, and M. Salierno, Acta Biomater. **38**, 106 (2016).
[7] J. Tomas and S. Kleinschmidt, Chem. Eng. Tech. **32**, 1470 (2009).
[8] S. Strauch and S. Herminghaus, Soft Matter **8**, 8271 (2012).
[9] K. Johnson, K. Kendall, and A. Roberts, Proc. R. Soc. London **324**, 301 (1971).
[10] E. Barthel, J. Phys. D **41**, 163001 (2008).
[11] A. J. Crosby, M. Hageman, and A. Duncan, Langmuir **21**, 11738 (2005).
[12] L. Leger and N. Amouroux, J. Adhes. **81**, 1075 (2005).
[13] M. Deruelle, L. Leger, and M. Tirrell, Macromolecules **28**, 7419 (1995).
[14] K. R. Shull, Mater. Sci. Eng., R **36**, 1 (2002).
[15] Y. Yu, D. Sanchez, and N. Lu, J. Mater. Res. **30**, 2702 (2015).
[16] M. K. Chaudhury and G. M. Whitesides, Langmuir **7**, 1013 (1991).
[17] E. Charrault, C. Gauthier, P. Marie, and R. Schirrer, Langmuir **25**, 5847 (2009).
[18] R. G. Horn, J. N. Israelachvili, and F. Pribac, J. Colloid Interface Sci. **115**, 480 (1987).
[19] C. Creton and M. Ciccotti, Rep. Prog. Phys. **79**, 046601 (2016).
[20] N. Amouroux, F. Restagno, and L. Léger, J. Adhes. **83**, 741 (2007).
[21] M. Deruelle, H. Hervet, G. Jandeau, and L. Léger, J. Adhes. Sci. Technol. **12**, 225 (1998).
[22] X. Zhu, E. Siamantouras, K. K. Liu, and X. Liu, J. Mech. Behav. Biomed. Mater. **56**, 77 (2016).
[23] M. Chyasnavichyus, S. L. Young, and V. V. Tsukruk, Jpn. J. Appl. Phys. **54**, 08LA02 (2015).
[24] H.-J. Butt, J. T. Pham, and M. Kappl, Curr. Opi. Colloid Interface Sci. **27**, 82 (2017).
[25] R. W. Style, C. Hyland, R. Boltyanskiy, J. S. Wettlaufer, and E. R. Dufresne, Nat. Commun. **4**, 2728 (2013).
[26] D. S. Rimai, D. J. Quesnel, and R. C. Bowen, Langmuir **17**, 6946 (2001).
[27] A. W. C. Lau, M. Portigliatti, E. Raphael, and L. Leger, Europhys. Lett. **60**, 717 (2002).
[28] C.-Y. Hui, T. Liu, T. Salez, E. Raphael, and A. Jagota, Proc. Royal Soc. A **471**, 20140727 (2015).
[29] X. Xu, A. Jagota, and C.-Y. Hui, Soft Matter **10**, 4625 (2014).
[30] T. Salez, M. Benzaquen, and É. Raphaël, Soft Matter **9**, 10699 (2013).
[31] J. Long, G. Wang, X.-Q. Feng, and S. Yu, Int. J. Solids Struct. **84**, 133 (2016).
[32] S. Karpitschka, L. van Wijngaarden, and J. H. Snoeijer, Soft Matter **12**, 4463 (2016).
[33] Z. Cao, M. J. Stevens, and A. V. Dobrynin, Macromolecules **47**, 3203 (2014).
[34] Z. Cao and A. V. Dobrynin, Langmuir **31**, 12520 (2015).
[35] See Supplemental Material at http://link.aps.org/supplemental/10.1103/PhysRevMaterials.1.015602 for experimental details and additional figures on materials characterization and data analysis.
[36] K. E. Jensen, R. Sarfati, R. W. Style, R. Boltyanskiy, A. Chakrabarti, M. K. Chaudhury, and E. R. Dufresne, Proc. Natl. Acad. Sci. USA **112**, 14490 (2015).
[37] K. R. Shull, D. Ahn, W.-L. Chen, C. M. Flanigan, and A. J. Crosby, Macromol. Chem. Phys. **199**, 489 (1998).
[38] M. D. Bartlett and A. J. Crosby, Langmuir **29**, 11022 (2013).
[39] G. M. Pharr and W. C. Oliver, MRS Bulletin **17**, 28 (1992).
[40] C.-Y. Hui, J. M. Baney, and E. J. Kramer, Langmuir **14**, 6570 (1998).
[41] D. Maugis and M. Barquins, J. Phys. D **11**, 1989 (2001).
[42] C.-Y. Hui, Y. Y. Lin, F.-C. Chuang, K. R. Shull, and W.-C. Lin, J. Polym. Sci. Part B: Polym. Lett. **44**, 359 (2006).
[43] Y.-Y. Lin and H.-Y. Chen, J. Polym. Sci. Part B: Polym. Lett. **44**, 2912 (2006).
[44] D. Maugis, Langmuir **11**, 679 (1995).
[45] P. G. De Gennes, Langmuir **12**, 4497 (1996).

[46] J. Ally, E. Vittorias, A. Amirfazli, M. Kappl, E. Bonaccurso, C. E. McNamee, and H. J. Butt, Langmuir **26**, 11797 (2010).
[47] H.-J. Butt and M. Kappl, *Surface and Interfacial Forces* (WILEY-VCH Verlag, Weinheim, 2010).
[48] J. M. Y. Carrillo and A. V. Dobrynin, Langmuir **28**, 10881 (2012).
[49] D. Quéré, Physica A **313**, 32 (2002).
[50] A. C. Kuo, in *Polymer Data Handbook*, edited by J. E. Mark (Oxford University Press, Oxford UK, 1999), pp. 411–435.
[51] J. B. Bostwick, M. Shearer, and K. E. Daniels, Soft Matter **10**, 7361 (2014).
[52] R. W. Style, R. Boltyanskiy, Y. Che, J. S. Wettlaufer, L. A. Wilen, and E. R. Dufresne, Phys. Rev. Lett. **110**, 066103 (2013).